Processing and Application of Ceramics 18 [2] (2024) 156–161
https://doi.org/10.2298/PAC2402156W

Preparation and properties of Eu^{3+} doped tungstate red phosphor powders

Yaping Wang [1,2,*], Anqin Liu [1], Zhijuan Li [1], Zhuo Wang [1], Yunxia Chen [3]

[1] *School of Mechanical and Electrical Engineering, Yantai Institute of Technology, Yantai, 264003, China*
[2] *Yantai Institute of Coastal Zone Research, Chinese Academy of Sciences, Yantai, 264003, China*
[3] *College of Life Sciences, Shandong Agricultural University, Taian, 271018, China*

Received 7 February 2024; Received in revised form 13 May 2024; Accepted 28 May 2024

Abstract

$NaY(WO_4)_2:Eu^{3+}$ phosphors were synthesized using high-temperature solid state method. The effects of Eu^{3+} doping concentrations on structure and photoluminescence properties of the powders were investigated. The results indicate that the pure $NaY(WO_4)_2:Eu^{3+}$ phase can be produced by calcining at 800 °C where Eu^{3+} doping does not alter the main phase structure. Eu^{3+} ions were successfully incorporated into the crystal lattice, replacing Y^{3+} at the B-site. This caused gradual shifts of the characteristic X-ray diffraction peaks to lower 2θ angles. Morphological characterization revealed that the sample particles had irregular polygonal shapes with sizes ranging from 100 to 300 nm. There was minimal variation in morphology among samples with different doping concentrations. The samples exhibited the characteristic spectral emission of Eu^{3+} and emitted red light at a wavelength of 616 nm when excited by 394 nm near-ultraviolet light. The luminescence intensity of the nanophosphor gradually increased with increasing Eu^{3+} doping concentration, reaching its maximum at a doping ratio of 0.6, followed by a decrease due to the concentration quenching. The quenching mechanism was analysed to be primarily dipole-dipole interaction, in accordance with the Dexter's theory of doping concentration. The luminescence positions of the phosphors slightly changed with varying Eu^{3+} doping concentrations, and the colour coordinates closely matched the standard value of the red colour in the National Television Standards Committee, confirming the stability of the obtained powders as red phosphors.

Keywords: *tungstate, Eu-doping, solid state synthesis method, photoluminescence, quenching mechanism*

I. Introduction

In recent years, the light emitting diode (LED) has emerged as the dominant light source in the market due to its environmentally friendly nature and high efficiency. However, one of the drawbacks of LED technology is the absence of a red phosphor, which results in low colour rendering index and high colour temperature. To address this issue, extensive research has been conducted to develop more efficient red phosphors. A promising approach involves utilizing alkaline earth metal tungstate and molybdate as a matrix and rare earth ions as activators. This method holds significant research value in finding a solution to the problem [1].

The tungstates and molybdates of alkaline earth metals are self-activated luminescent materials with a wide transparency region (0.3–5 μm). They can be easily prepared and exhibit excellent chemical and thermal stability. Additionally, they can be doped with rare earth ions, making them effective phosphor excitation mediums [2,3]. These materials have gained significant attention and found applications in solid-state lighting [4], anti-counterfeiting [5,6], biological detection [7,8], temperature sensing [9] and other areas. One notable example is $NaY(WO_4)_2$, an ABO_4-type yttrium sodium tungstate, which offers several advantages such as high doping concentration, low fluorescence quenching, high conversion efficiency, low threshold and good stability. As a result, it finds extensive use in areas like human eye safety, optical communication, medical treatment and remote sensing [10]. Yao *et al.* [11] successfully synthesized $NaY(WO_4)_2:Er^{3+}$ phosphors through high-temperature solid state reaction. These phosphors exhibited strong green and red emissions. The researchers

* Corresponding author: tel: +86 13505357945
e-mail: *wangyaping@yitsd.edu.cn, fh20210406@126.com*

discovered that every emitted green and red photon required the involvement of at least two infrared photons. Furthermore, $NaY(WO_4)_2$:Er^{3+}/Yb^{3+} tungsten silicate glass ceramics were synthesized using the melting crystallization method [12]. These ceramics displayed strong green light emission when excited by a 980 nm laser. The researchers also synthesized a series of $NaY(WO_4)_2$:Sm^{3+} phosphors with different concentrations of Yb^{3+} as sensitizers [13]. These phosphors exhibited a strong green and weak red up-conversion emission, demonstrating their promising technological potential. Overall, $NaY(WO_4)_2$ has proven to be a reliable luminescent powder matrix.

Rare earth Eu^{3+} ions, with their unique $^4f_6$ shell layer structure, are commonly used as the luminescent centre in red fluorescent materials. This is because they efficiently emit red light when excited by ultraviolet light. The emission spectra lines correspond to the $^4f_6$ electronic transitions from the excited state $^5D_0$ energy level to the ^7F_J energy level. The shielding of the *f-f* transitioning electrons by the outer $^5s_2$ and $^5p_6$ electrons allows them to remain unaffected by the crystal field and other environmental influences, resulting in the formation of a linear emission spectrum [14,15].

Eu^{3+} doped $NaY(WO_4)_2$ red phosphors have been gaining attention due to the similar valence of Eu^{3+} and Y^{3+} and the small difference in atomic radii. This similarity has minimal impact on the structure and main properties of the $NaY(WO_4)_2$ matrix. Liu *et al.* [16] synthesized $NaY(WO_4)_2$ nanomaterials doped with Eu^{3+} and Tb^{3+} using a hydrothermal method. They discovered that $NaY(WO_4)_2$ phosphors activated by a single rare earth ion exhibited excellent emission properties in their respective regions when excited at either 246 or 230 nm. These findings suggest that the materials have potential applications in solid state lighting. Shi *et al.* [17] successfully synthesized a series of Eu^{3+}:$NaY(WO_4)_2$ red luminescent powders through a hydrothermal reaction. These powders exhibited desirable red chrominance in the International Commission on illumination (CIE) Chromatic coordinates when excited by near-ultraviolet (UV) light and near-infrared light. The analysis based on the G. Blasse's theory and the Dexter's theory revealed that the energy transfer mechanism between Eu^{3+} ions was primarily governed by the multipolar interactions of the electric dipole-dipole (*d-d*) interactions. Du *et al.* [18] synthesized a series of novel $Na(La_xEu_yY_{1-x-y})(WO_4)_2$ red luminescent powders using a high-temperature solid-state method. Their research showed that the introduction of La^{3+} ions resulted in changes to the length of the W−O bond and the matrix lattice, which in turn altered the energy transfer mechanism of the phosphor. This confirms that the regulation of red emission can be achieved through La^{3+} doping.

Despite the existing reports, further research is needed to address the shortage of red phosphors. Currently, there is a lack of comprehensive studies on the optical properties of $NaY(WO_4)_2$ red phosphors doped with various concentrations of Eu^{3+} under UV excitation. This study aims to systematically prepare $NaY(WO_4)_2$-based red luminescent powders with different concentrations of Eu^{3+} using the traditional high-temperature calcining method. The molar ratios of Y_2O_3 and Eu_2O_3 raw materials were adjusted accordingly. The samples were analysed for their structure and luminescence properties using X-ray diffraction (XRD), scanning electron microscope (SEM) and photoluminescence (PL). Furthermore, the study discussed the luminescent performance and provided a mechanistic analysis of phosphors under UV excitation, offering empirical evidence for the fabrication of high-quality red luminescent powders.

II. Experimental

Tungstate powders were synthesized using compounds of the constituent elements: Na_2CO_3 (AR ≥ 99.5%), WO_3 (AR ≥ 99%), Y_2O_3 (99.9% metals basis) and Eu_2O_3 (99.9% metals basis), all obtained from Shanghai Macklin Biochemical Technology Co. Ltd. The stoichiometric amounts of the precursor compounds (based on following $NaY_{1-x}(WO_4)_2$:xEu^{3+} composition, where x = 0.1, 0.2, …, 0.9) were thoroughly blended by ball milling for 2 h to create a homogeneous mixture. The mixtures were heated to 800 °C for 4.5 h to complete crystallization. After natural cooling to room temperature, the calcined mixtures were ground for 0.5 h in an onyx mortar to obtain the final samples.

XRD patterns of the samples were recorded using a Shimadzu XRD-6100 X-ray diffractometer equipped with a Cu anode target (λ = 0.15406 nm). The instrument was operated at 40 kV and 30 mA, with a scanning speed of 10 °/min. Morphology characterization and energy-dispersive X-ray spectroscopy (EDS) analysis of the samples were conducted using a Hitachi S-4800 scanning electron microscope. The particle sizes of the powder were measured using a Malvern Zetasizer Nano-ZS90 laser particle size analyser (ZEN3590, UK). For emission spectra the scanning wavelength range was set from 200 to 700 nm, while for excitation spectra the scanning wavelength range was set from 320 to 500 nm. Both spectra were measured using a Hitachi F-4700 fluorescence spectrometer. All tests were performed at room temperature.

III. Results and discussion

3.1. XRD structural characterization

Figure 1 presents XRD patterns of the synthesized samples doped with different amounts of Eu^{3+}. The obtained samples show similar patterns lines and diffraction peaks that align well with the characteristic diffraction peaks of the tetragonal phase $NaY(WO_4)_2$ (standard card JCPDS# 48-0886). No additional phases were detected, indicating that the prepared samples maintain

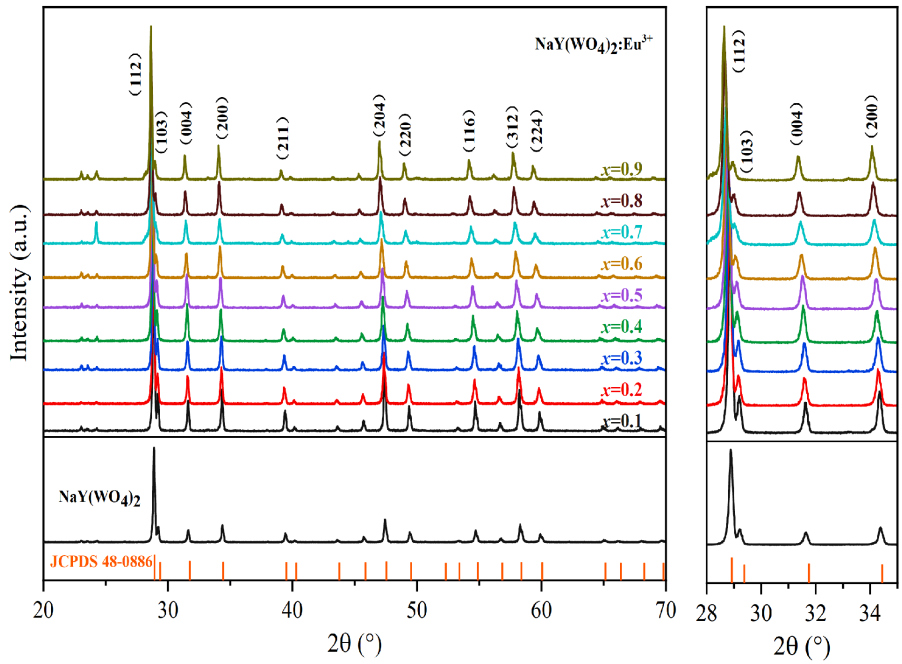

Figure 1. XRD patterns of the synthesized samples with different Eu^{3+} concentrations

their tetragonal scheelite structure even after Eu^{3+} doping. The main diffraction peaks were sharp and intense, suggesting the high crystallinity of the obtained samples. Calcining at 800 °C successfully produces pure-phase Eu^{3+}-doped tungstate red phosphors, which is consistent with the findings observed in other rare earth ion doping processes [19].

With the increasing concentration of Eu^{3+} doping, the characteristic diffraction peaks, such as (112), show a tendency to gradually shift towards lower 2θ angles. This phenomenon can be attributed to the difference in ionic radius between Y^{3+} (0.090 nm) and Eu^{3+} (0.095 nm). As more Y^{3+} sites are replaced by Eu^{3+} ions of the same valence, the interplanar spacing widens, leading to the lattice expansion according to the Bragg's formula $\lambda = 2d \cdot \sin\theta$. Consequently, the diffraction peaks shift to lower angles, indicating the successful doping of Eu^{3+} ions into the lattice.

3.2. Morphology characterization

SEM micrographs of the synthesized samples doped with various concentrations of Eu^{3+} are shown in Fig. 2. It can be seen that particle sizes of the samples are relatively uniform, with clear and smooth surfaces. The particles exhibit irregular polygonal shapes, indicating successful crystallization. The particle sizes were measured to be in the nanoscale range, i.e. from 100 to 300 nm (Table 1). Some particles tend to agglomerate due to the high temperature reaction, small particle size, large specific surface area and high surface energy. However, the morphology remains consistent across different samples, suggesting that the dopant ions did not affect the phase formation of the samples. The presence of Na, Y, W, O and Eu elements in $NaY(WO_4)_2$ is confirmed by the EDS spectrum shown in Fig. 3.

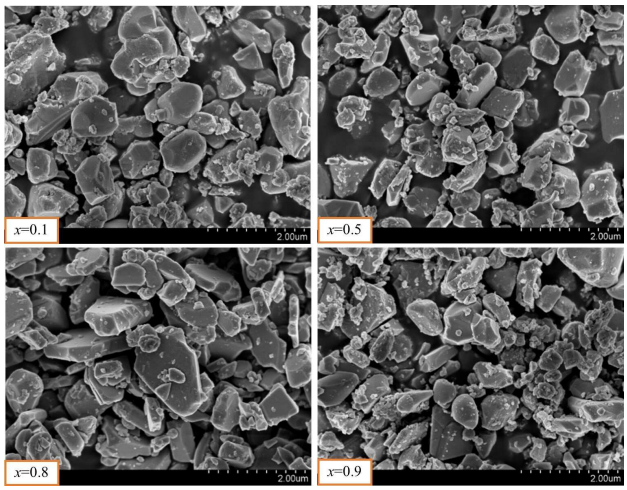

Figure 2. SEM micrographs of the synthesized samples (x = 0.1, 0.5, 0.8 and 0.9)

Table 1. Particle size distribution of the synthesized samples (x = 0.1, 0.5, 0.8 and 0.9)

Samples	Average particle size [nm]	*PdI*
$x = 0.1$	228	0.036
$x = 0.5$	86.1	0.259
$x = 0.8$	97.0	0.236
$x = 0.9$	227	0.128

3.3. Photoluminescence properties

Figure 4 illustrates the excitation spectrum of the synthesized powders, monitored at a wavelength of 615 nm. The spectrum reveals sharp peaks at 320, 363, 383, 394, 417 and 467 nm, corresponding to the $^7F_0 \rightarrow {}^5H_6$, $^7F_0 \rightarrow {}^5D_4$, $^7F_0 \rightarrow {}^5L_7$, $^7F_0 \rightarrow {}^5L_6$, $^7F_0 \rightarrow {}^5D_3$ and $^7F_0 \rightarrow {}^5D_2$ transitions, respectively [20]. These transitions align with the characteristic $4f$-$4f$ transitions of Eu^{3+} (re-

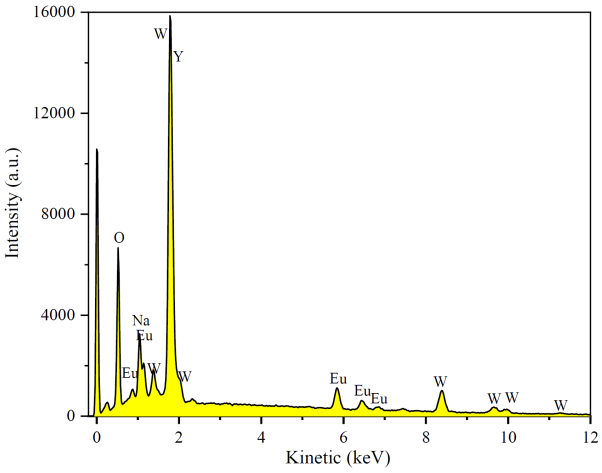

Figure 3. EDS spectrum of the synthesized sample $x = 0.5$

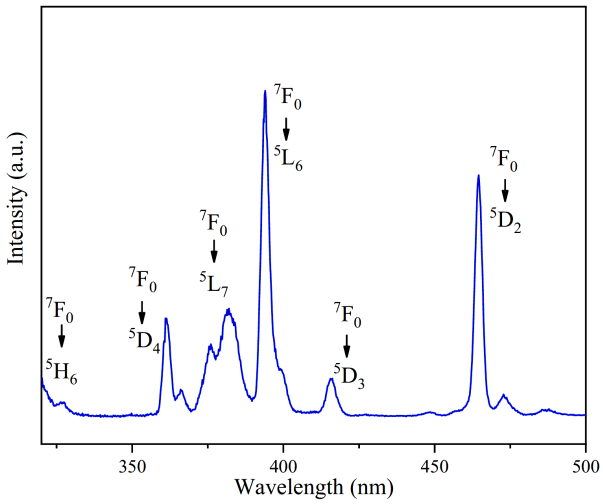

Figure 4. Excitation spectrum of the synthesized powders at the monitoring wavelength of 615 nm

ferred to as the characteristic excitation band) [21]. Notably, the peaks at 394 nm ($^7F_0 \rightarrow {}^5L_6$) and 467 nm ($^7F_0 \rightarrow {}^5D_2$) are particularly prominent and coincide with the wavelengths of commercially available near-ultraviolet light and blue LED chips [22], respectively. This suggests that the obtained samples are red luminescent powders suitable for UV or near-ultraviolet excitation.

As shown in Fig. 5, the phosphors emit red light at a wavelength of 616 nm when excited by 394 nm near-ultraviolet light. This emission can be attributed to the electric dipole transition of Eu^{3+} ($^5D_0 \rightarrow {}^7F_2$) [23]. The positional distributions of the emission spectra remain relatively unchanged after doping with different proportions of Eu^{3+} ions. However, the intensities of the emitted light do exhibit significant changes. As the concentration of Eu^{3+} doping increases, the luminous intensity of the samples gradually enhances and reaches its peak at a doping ratio of 0.6. However, further increase in Eu^{3+} doping concentration leads to a decrease in luminescence intensity and concentration quenching occurs. According to the Dexter's theory of doping concentration, multipolar interactions are the main mechanism responsible for this quenching phenomenon [16].

The type of multipolar interactions can be analysed using formulas (Eqs. 1 and 2) from the Dexter's theory [24]:

$$I \propto a^{\left(1-\frac{s}{d}\right)} \cdot \Gamma\left(1+\frac{s}{d}\right) \tag{1}$$

$$a = C\Gamma\left(1-\frac{d}{s}\right)\left[x_0\left(1+\frac{A}{\gamma}\right)\right]^{\frac{d}{s}} \tag{2}$$

These formulas include constants x_0 and A, where γ represents the intrinsic transition probability of the activator. Additionally, d corresponds to the dimension of the prepared samples, and s represents the series of elec-

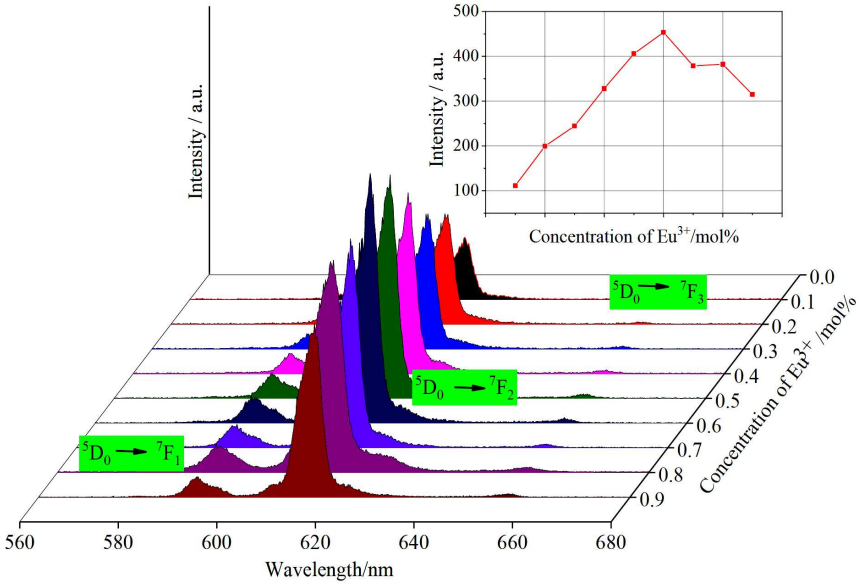

Figure 5. Emission spectra of $NaY(WO_4)_2$ phosphors doped with different Eu^{3+} concentrations (λ_{ex} = 394 nm)

Table 2. The NTSC colour coordinates of the doped samples

Molar ratio, x	0.1	0.2	0.3	0.4	0.5	0.6	0.7	0.8	0.9
Color coordination, X	0.5636	0.6045	0.6083	0.6289	0.63	0.6373	0.6418	0.6369	0.6295
Color coordination, Y	0.3434	0.3399	0.3382	0.34	0.335	0.3345	0.3358	0.3356	0.3344

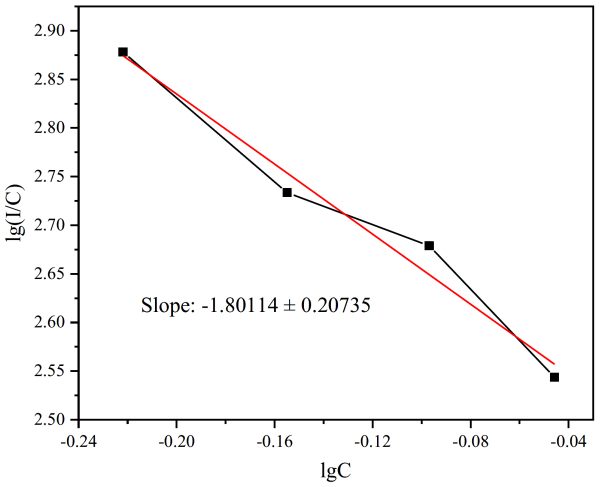

Figure 6. Logarithmic relationship between luminescence intensity and concentration of powders with doping ratios higher than 0.5

tric multipolar interactions. The series can have values of 6, 8 and 10, which respectively refer to the dipole-dipole (d-d) interaction, the dipole-quadrupole (d-q) interaction, and the electric quadrupole-quadrupole (q-q) interaction.

Figure 6 depicts the molar concentration dependence of luminescence intensity, illustrating the relationship between the emission intensity (I) and the doping concentration (C) for powders with doping ratios higher than 0.5. The slope ($-s/d$) of the curve obtained by fitting is about −1.8. Here, d takes the value of 3 and s was calculated to be 5.4, which is remarkably close to the electric multipole exponent 6 for the electric dipole-electric dipole interaction, suggesting that the type of multipolar interactions leading to the concentration quenching are electric dipole-dipole interactions.

The colour coordinates of the doped samples with different Eu^{3+} concentrations are listed in Table 2. The luminescence positions of the phosphors slightly change with varying Eu^{3+} doping concentrations, but they still fall within the red region. The colour coordinates closely match the standard value of the red colour in the National Television Standards Committee (NTSC: 0.670, 0.330), confirming the stability of the obtained powders as red phosphors. Figure 7 illustrates the CIE coordinates of the phosphor sample with the doping ratio of 0.7.

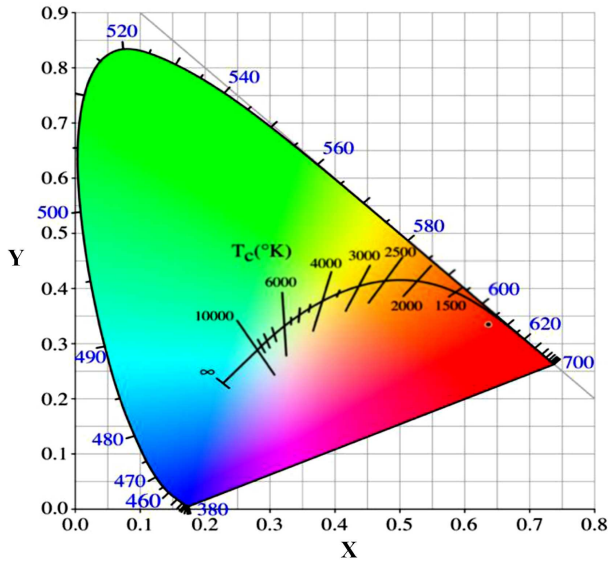

Figure 7. CIE of the phosphor sample x = 0.7

IV. Conclusions

A pure $NaY(WO_4)_2$:Eu^{3+} phase with a tetragonal scheelite structure can be synthesized using the high-temperature solid state method at a calcining temperature of 800 °C. Eu^{3+} doping does not change the main phase structure and Eu^{3+} was successfully incorporated into the crystal lattice, replacing Y^{3+} at the B-site. The powders exhibit irregular polygonal shapes under the electron microscope, with particle sizes ranging from 100 nm to 300 nm. Upon excitation, the samples exhibit the characteristic spectrum of Eu^{3+}, with the strongest peaks observed at 394 nm ($^7F_0 \rightarrow {}^5L_6$) and 467 nm ($^7F_0 \rightarrow {}^5D_2$). This indicates that the synthesized red luminescent powders are suitable for excitation by ultraviolet or near-ultraviolet light.

Under the excitation of 394 nm near-ultraviolet light, the phosphors emit red light at a wavelength of 616 nm. As the concentration of Eu^{3+} doping increased, there was a slight shift in the luminous positions of the phosphors, and the colour coordinates approached the standard value for the red colour in NTSC. Additionally, the luminescence intensities of the samples gradually increased and reached their maximum at a doping ratio of 0.6. Subsequently, the intensities decreased due to the concentration quenching. According to the Dexter's theory of doping concentration, the main mechanism for this quenching was the electric dipole-dipole interaction in the multipolar interaction.

Acknowledgements: This work was supported by the Funding for Teachers' Study Visit and Training from Provincial Ordinary Undergraduate Colleges and Universities in Shandong Province.

References

1. C.L. Ranganatha, B.S. Palakshamurthy, G.P. Abhilash, A. Mathew, H.M. Suresh Kumar, C. Shivakumar, "De-

velopment of flexible luminescent films, photoluminescence properties and anti-counterfeiting applications of $SrMoO_4$:Tb^{3+} green phosphors", *J. Mater. Sci. Mater. Electron*., **34** (2023) 1412.
2. W.F. Rao, Y. Guan, J.Y. Yang, Q.Q. Huang, J.H. Miao, "Fabrication, characterization, and luminescent properties of Y_2WO_6: Gd^{3+}, Dy^{3+} hierarchical microspheres", *J. Mater. Sci. Mater. Electron*., **30** (2019) 4393–4399.
3. N.R. Aghamalyan, R.B. Kostanyan, R.K. Hovsepyan, "Luminescent properties of Nd^{3+} ions in $Pb(MoO_4)_x(WO_4)_{1-x}$ crystals", *J. Contemp. Phys*., **53** (2018) 41–47.
4. J.Y. Su, X.Y. Zhang, X. Li, M.L. Qu, "Synthesis and luminescence properties of Yb^{3+}, Tm^{3+} and Ho^{3+} co-doped $SrGd_2(WO_4)_2(MoO_4)_2$ nano-crystal", *Adv. Powder Technol*., **31** [3] (2020) 1051–1059.
5. X. Zhao, S. Chen, C. Ye, L. Li, Y. Hu, X. Wang, Y. Song, "Triplet-triplet annihilation upconversion combined with afterglow phosphors for multi-dimensional anti-counterfeiting and encoding", *J. Mater. Chem. C*, **10** [35] (2022) 12853–12862.
6. I. Ayoub, R. Sehgal, V. Sharma, R. Sehgal, H.C. Swart, V. Kumar, "Rare-earth doped inorganic materials for light-emitting applications", pp. 1–30 in *Advanced Materials for Solid State Lighting. Progress in Optical Science and Photonics Vol. 25*. Eds. V. Kumar, V. Sharma, H.C. Swart, Springer, Singapore, 2023.
7. B. Kaur, R. Kumar, S. Chand, K. Singh, A. Kumar Malik, "Determination of norfloxacin in urine and pharmaceutical samples using terbium doped zinc sulphide nanomaterials-sensitized fluorescence method", *Spectrochim. Acta A*, **214** (2019) 261–268.
8. H. Peng, D. Zhang, J. Hu, "Synthesis of a novel magnetic-luminescent bifunctional imaging materials by introducing WO_{3-x} interlayer", *Appl. Phys. A*, **125** (2019) 827.
9. M. Maimaiti, L. Wang, A. Xiakeer, M. Jiang, X. Feng, "Er^{3+} and Yb^{3+} codoped Bi_2WO_6 upconversion luminescent material preparation and temperature sensing properties", *J. Mater. Sci. Mater. Electron*., **34** (2023) 1911.
10. J. Ma, X. Sun, Y. Li, X. Zhang, Y. Li, H. Liu, D. Huang, H. Zhu, H. Qi, C.K. Mahadevan, "Structural and optical properties of $NaY(WO_4)_2$:Tm^{3+}, Yb^{3+} and $NaY(WO_4)_2$:Tm^{3+},Er^{3+},Yb^{3+} powders synthesized by the high-temperature solid-state method", *J. Mater. Sci. Mater. Electron*., **33** (2022) 2949–2956.
11. H. Yao, H. Shen, Q. Tang, N. Yang, Z. Zhai, Y. Li, "Influence of Er^{3+} doping concentration and temperature on upconversion photoluminescence property of $NaY(WO_4)_2$ phosphor", *Appl. Phys. A*, **124** (2018) 467.
12. Q. Wei, C. Ma, M. Zhao, G. Ren, C. Su, "Preparation and up-conversion luminescence of $NaY(WO_4)_2$:Er^{3+}/Yb^{3+} glass ceramics under different heat treatment conditions", *J. Aust. Ceram. Soc*., **58** (2022) 1053–1060.
13. Z. Zhou, X. Shi, Z. Leng, X. Jiang, W. Yang, H. Liu, H. Sha, T. Zhang, Y. Li, S. Li, H. Hu, C. Li, F. Zeng, "Yb^{3+} induced highly efficient green up-conversion emission of $NaY(WO_4)_2$:Sm^{3+} phosphors", *J. Mater. Sci. Mater. Electron*., **33** (2022) 25796–25804.
14. C.R. Ronda, T. Justel, H. Nikol, "Rare earth phosphors: Fundamentals and applications", *J. Alloys Compd*., **275** (1998) 669–676.
15. P. Dang, G. Li, X. Yun, Q. Zhang, D. Liu, H. Lian, M. Shang, J. Lin, "Thermally stable and highly efficient red-emitting Eu^{3+}-doped $Cs_3GdGe_3O_9$ phosphors for WLEDs: non-concentration quenching and negative thermal expansion", *Light Sci. Appl*., **10** (2021) 29.
16. Y. Liu, G. Liu, J. Wang, X. Dong, W. Yu, T. Wang, "Hydrothermal synthesis, multicolor tunable luminescence and energy transfer of Eu^{3+} or/and Tb^{3+} activated $NaY(WO_4)_2$ nanophosphors", *J. Mater. Sci. Mater. Electron*., **27** (2016) 10780–10790.
17. Z. Shi, J. Wang, H. Jiang, X. Guan, Y. Lu, J. Shi, "Photoluminescence characteristics and energy transfer mechanism of Eu^{3+}:$NaY(WO_4)_2$ microparticles", *J. Mater. Sci. Mater. Electron*., **30** (2019) 3169–3176.
18. Q. Du, A. Du, B. Yang, G. Zheng, C. Guo, J. Zou, "Synthesis and characterization of red emission phosphor $NaY(WO_4)_2$:Eu^{3+} with La^{3+}-doped", *J. Mater. Sci. Mater. Electron.*, **33** (2022) 13207–13216.
19. C. Zhang, X. Wang, C. Li, H. Lin, Z. Su, "Effect of Li ions on structure and spectroscopic properties of $NaY(WO_4)_2$: Yb/Ho phosphor", *Ceram. Int*., **46** (2020) 24248–24256.
20. P. Du, X. Huang, J.S. Yu, "Facile synthesis of bifunctional Eu^{3+}-activated $NaBiF_4$ red-emitting nanoparticles for simultaneous white light-emitting diodes and field emission displays", *Chem. Eng. J*., **337** (2018) 91–100.
21. C.M. Mehare, Y.R. Parauha, V. Chopra, S. Ray, N.S. Dhoble, C. Ghanty, S.J. Dhoble, "Tailoring the luminescent properties of $Ca_9La(PO_4)_5(SiO_4)F_2$: 1mol%Eu^{3+} phosphor via doping of chloride, molybdate, vanadate, sulfate, and tungstate ions", *J. Mater. Sci. Mater. Electron*., **31** (2020) 3426–3440.
22. J.W. Chung, H.K. Yang, B.K. Moon, "Double-perovskite Ca_2LaNbO_6:Mn^{4+} deep red phosphors used to improve the color rendering index properties of WLED", *J. Korean Phys. Soc*., **81** (2022) 885–893.
23. J. Shen, Z.X. Wang, J. Zhou, X. Liu, W. Chen, "Photoluminescence properties of NUV light excited $Ba(Mg_{1/3}Nb_{2/3})O_3$: Eu^{3+} red phosphor with high color purity", *Ceram. Int*., **45** (2019) 11844–11849.
24. S. Devi, S. Kaushik, M. Kumar, H. Dalal, S. Gaur, S. Kumar, "Influence of Eu^{3+} doping on crystallographic and photophysical aspects of combustion synthesized $BaSrY_4O_8$ nanophosphor for photoelectronic appliances", *Appl. Phys. A*, **128** (2022) 23.